Published in final edited form as:

J Immunol. 2012 November 15; 189(10): 4981–4988. doi:10.4049/jimmunol.1202017.

FcγRIIb on liver sinusoidal endothelium clears small immune complexes

Latha P. Ganesan[*], **Jonghan Kim**[†], **Yun Wu**[‡], **Sudhasri Mohanty**[*], **Gary S. Phillips**[§], **Daniel J. Birmingham**[*], **John M. Robinson**[¶], and **Clark L. Anderson**[*]

[*]Department of Internal Medicine, The Ohio State University, Columbus, OH, 43210, USA

[§]Department of Biostatistics, The Ohio State University, Columbus, OH, 43210, USA

[¶]Department of Physiology and Cell Biology, The Ohio State University, Columbus, OH, 43210, USA

[‡]NSF Nanoscale Science and Engineering Center for Nanoengineering of Polymer Biomedical Devices, The Ohio State University, Columbus, OH, 43210, USA

[†]Harvard School of Public Health, Boston, MA, 02115, USA

Abstract

It has long been known that the ITIM-bearing IgG Fc receptor (FcγRIIb, RIIb) is expressed on liver sinusoidal endothelial cells (LSEC) and that the liver is the major site of small immune complex (SIC) clearance. Thus, we proposed that RIIb of LSEC eliminates blood-borne small immune complexes (SIC), thereby controlling IC-mediated autoimmune disease. Testing this hypothesis we found most RIIb of the mouse, fully three-quarters, to be expressed in liver. Moreover, most (90%) liver RIIb was expressed in LSEC, the remainder in Kupffer cells (KC). An absent FcRγ in LSEC implied that RIIb is the sole FcγR expressed. Testing the capacity of liver RIIb to clear blood-borne SIC we infused mice intravenously with radioiodinated SIC made of ovalbumin and rabbit IgG anti-ovalbumin. Tracking decay of SIC from the blood, we found the RII KO strain to be severely deficient in eliminating SIC compared with the WT strain, terminal half-lives being, respectively, 6 and 1.5 hours. RIIb on LSEC, a major scavenger, keeps SIC blood concentrations low and minimizes pathologic deposition of inflammatory IC.

Keywords

Endocytosis; pinocytosis; reticuloendothelial system; mononuclear phagocyte system; IgG; antibody; Fc receptors; CD32; FcγR; Kupffer cells; SLE; glomerulonephritis; autoimmune disease

INTRODUCTION

It is an axiomatic function of the immune system that complexes of antigen and antibodies are eliminated efficiently from the blood stream, ridding the body of harmful elements of a

CORRESPONDING AUTHOR: Dr. Clark L. Anderson, Dept. of Internal Medicine, The Ohio State University, 012K Davis Heart and Lung Research Institute, 473 West Twelfth Avenue, Columbus, OH 43210. Phone: (614) 247-7650; Fax: (614) 247-7669; anderson.48@osu.edu; www.andersonlab.com.

variety of sorts, both invasive and endogenous. A number of features of immune complexes govern their elimination, the most obvious being size. Large immune complexes composed of, for example, bacteria-sized microorganisms and blood cells coated with antibody are removed by cells of the mononuclear phagocyte system by the process of receptor-mediated phagocytosis. These complexes are sometimes referred to as ‘insoluble’ because they readily sediment at low gravity forces.

Likewise, small immune complexes (SIC), the size of serum proteins complexed with corresponding antibody, are in most situations eliminated efficiently from the blood, specifically by the cells of the classical reticuloendothelial system, chiefly by the sinusoidal cells of the liver(1–4). These SIC are often termed ‘soluble’ because they fail to sediment at low gravity forces; experimentally they are prepared at ‘antigen excess’, at concentrations of antigen exceeding that required for the optimal preparation of insoluble immune complexes(5). In certain circumstances, however, these SIC fail to be eliminated and go on to produce disease. The pathophysiology of such immune complex-mediated diseases has been the focus of considerable experimental interest over the last century. Intensive study of the mechanisms of these diseases, beginning with experimental models of serum sickness in the 1950s most prominently by Dixon(6) and Benacerraf(7) and others, has led to the current concept that SIC must accrete to a certain requisite size in order to deposit in critical organs, such as the kidney, where they produce inflammation and disease(8–11). Thus, analyzing the mechanism by which immune complexes, while still small, are eliminated by the liver becomes an imperative theoretical and practical objective.

A crucial clue to the mechanism of SIC elimination emerged 30 years ago when it was observed that mab 2.4G2, specific for the binding sites of all mouse FcγR, blocked liver uptake of SIC infused intravenously into mice(3). This finding implicated liver sinusoidal FcγR in the elimination of SIC. Many concluded that the Kupffer cells (KC) were responsible for such liver elimination. Rather, as we have recently found, liver sinusoidal endothelial cells (LSEC) expressing FcγRIIb (RIIb) are responsible for virtually all mab 2.4G2 binding in mouse liver(12). Several converging lines of recent evidence (4, 12–18) now indicate that the predominant FcγR on LSEC is RIIb, the low affinity ITIM-bearing inhibitory receptor studied most carefully on B cells, macrophages, and dendritic cells (reviewed) (19, 20).

We are led by the evidence presented above to propose that RIIb expressed on LSEC are responsible for the ongoing removal of SIC from the blood. This hypothesis has two predictions; first, that liver expression of RIIb is remarkably abundant and, second, that a mouse strain lacking RIIb will fail to remove SIC from blood. We tested these two predictions, the first by immunofluorescence microscopy and immunoblotting, measuring the expression of RIIb in liver compared with the entire animal; and the second by comparing the rates of elimination of radioiodinated SIC from the blood in WT and RIIb KO strains of mice.

Neither test rejected the hypothesis. Rather, a very high fraction, fully three-quarters, of total body RIIb was found in the liver, most on LSEC. Further, the removal rate of SIC from blood of RIIb KO mice when compared with WT mice was severely curtailed. These results

confirm our hypothesis and suggest new ways of conceptualizing and treating immune complex mediated diseases.

METHODS

Ethics statement and animals

Male mice of age 12–15 weeks were obtained from Taconics Laboratory. They were of strains BALB/c wild type (WT) and FcγRIIb (RIIb) knock out (KO) on a BALB/c background (C.129S4 (B6)-*Fcgr2b*^{tm1TtK}/cAnNTac N12C.129S4 and model number 580-M). The RIIb KO mice were generated and described previously (21). All protocols were approved by The Ohio State University Institutional Animal Care and Use Committee. Bleedings were performed under Isoflurane anesthesia, and all efforts were made to minimize suffering.

Cells

Raw 264.7, A20, and COS-7 cells were obtained from American Type Culture Collection. COS-7 cells were maintained in Dulbecco's modified Eagle's medium supplemented with 10% fetal bovine serum. Raw 264.7 and A20 were maintained in RPMI 1640 medium supplemented with 5% fetal bovine serum. BMM (bone marrow macrophages) were obtained and differentiated with M-CSF as previously described(22).

Quantitative Immunoblot

The expression of RIIb and Syk in various organs was quantified by immunoblot as follows: Organs (kidney, spleen, ileum, liver, heart, spleen and lung) from 3 sacrificed mice were removed and weighed. Small pieces of about 100μg from each organ were homogenized with a glass homogenizer in a lysis buffer composed of 25mM HEPES, 20mM $Na_4H_2O_7.10H_2O$, 100mM NaF, 4mM EDTA, 2mM Na_3VO_4, 1% Triton X-100, 0.34mg/ml PMSF, 0.01mg/ml aprotinin, and 0.01mg/ml leupeptin. Lymph nodes (LN) from axillary, mesangial, inguinal, and sub-mandibular regions were pooled. Bone marrow cells (BMC) were flushed from femurs, centrifuged at 376×g for 5 min, and lysed. Blood (~80μl) was obtained from 3 mice via the retro-orbital plexus using heparinized capillary pipettes, and the erythrocytes were lysed by incubation in dilute saline (PBS/50 in water) at room temperature for 10 min. Cells remaining were spun down at 376×g for 5 min and lysed. All lysates were incubated on ice for 30 min and centrifuged at 18,407×g for 15 min. The protein concentrations of spun lysates were estimated using the BCA protein assay.

Organ lysates (35μg) along with lysates of control standards (0, 3, 6, 9, and 12μg of lysates from A20 cell line for RIIb blots and 0, 5, 10, 15, 20μg of lysates from RAW 264.7 cells for Syk blots) were separated on 8–16% gradient SDS-polyacrylamide gels, and the proteins were transferred to nitrocellulose membranes (0.45μm). The membranes were blocked with 5% milk for 30 min and then incubated overnight with primary rabbit anti-mouse RIIb (kind gift from John Cambier) and rabbit anti-Syk (Santa Cruz) antibodies at concentrations of 1:5000 at 4°C. The bands were developed using Alexa 488 fluor-conjugated goat anti-rabbit IgG antibody at a concentration of 1:1000 and detected for quantification using a laser scanner (Pharos-FX, Bio-Rad).

Band intensities were quantified using Quantity One software from Bio-Rad. The RAW and A20 cell-equivalent concentrations of RIIb and Syk, respectively, were calculated from standard curves after subtracting background. The total amounts of RIIb and Syk in all organs were calculated by factoring the weights of the respective organs and the respective volumes of lysis buffer and were plotted as percentages of total after normalizing to the organ with the lowest signal within each experiment. For statistical analysis protein expression was natural log-transformed to normalize the distribution and to stabilize the variance across organ type (homoscedasticity assumption). Using a mixed-effects linear regression model where the subject is the random effect and the organ type is the fixed effect we compared the RIIb protein expression in the liver to the average of the other 8 organs. Similarly, we compared the Syk protein expression in the spleen to the average of the other 8 organs.

Equal protein loading of all organ lanes was assured by the following strategies: First, equal amounts of protein lysates (BCA assay) were loaded into each gel well. Second, densitometry of the Coomassie Blue-stained gel showed that total densities of all bands in an organ lane except blood were no more than 2-fold different than the mean organ density, and blood was 3.4x less than the mean. Third, re-blotting the immunoblot from Figure 1 with goat anti-actin antibody (Santa Cruz Biotechnology, Inc) and analyzing the actin bands by densitometry using Image J software, showed that, save for the blood sample where actin was present but low, the density of the actin bands from any of the organs was less than two-fold different from the mean density of all actin bands. The literature records similar variation to ours when comparing organs (23–25). Erythrocyte ghost proteins are known to stain poorly with Coomassie (26).

For visual representation alone (Fig. 1A), as opposed to quantification (Fig. 1B), 50μg of tissue lysates were separated on 10% linear SDS-polyacrylamide gels, transferred, probed with antibody, developed by enhanced chemiluminescence (ECL), and imaged. The lysates from cell lines A20, RAW 264.7, and bone marrow macrophages differentiated using M-CSF were used as control sources of b1 and b2 protein isoforms.

Immunofluorescence

Small pieces of liver (~5mm) were fixed in 4% paraformaldehyde in PBS for 2 hrs at room temperature and, after washing with PBS, were infused in 20% sucrose-PBS overnight at 4°C. The tissues were then embedded in a freezing medium and stored at −80°C. Cryostat sections, 5μm thickness, were blocked in 5% milk-PBS prior to incubation overnight at 4°C with primary antibodies. The primary antibodies rabbit anti-mouse RIIb, goat anti-mouse RIIb (kind gift from Mark Coggeshall), rabbit anti-mannose receptor (Santa Cruz), and rabbit anti-FcRγ-chain (Millipore, MA, USA) antibody were all used at dilutions of 1:25. The mab 2.4G2 was used at a concentration of 20μg/ml. After 3 washes with PBS the sections were incubated with secondary antibodies for 1hr at room temperature. Nuclei were stained with DAPI for 10 min, and the sections were mounted under cover slips in Prolong gold (Invitrogen). Control incubations included isotype controls along with their respective secondary antibodies and also secondary antibodies alone. The images were acquired in the Olympus FluoView 1000 Laser Scanning Confocal microscope equipped with a spectral

detection system for a finer separation of fluorochromes (FV 1000 spectra) using 60x oil immersion lens at room temperature. Image analyses were done using FluoView software (Olympus version 2.1.39). In Fig. 4, to overcome the inherent limits of resolution in the z-dimension in our confocal microscopes, we used ultrathin cryosections of liver tissue as the substratum for high-resolution immunofluorescence microscopy as we have described (27–29). Preparation of tissue and ultrathin cryosections we described in detail earlier (30).

Quantitative Microscopy

The relative liver expression of RIIb between LSEC and KC, shown in Fig. 3 (bottom row), was quantified from merged immunofluorescence images dual-stained for RIIb (green) using goat anti-RIIb antibody and anti-F4/80 (red) in the following manner. The total intensity of RIIb (green) in the images was calculated using Image J software. From this total was subtracted the intensity of RIIb measured in all cropped KC, identified with F4/80. Thus, total intensity of RIIb minus KC intensity of RIIb equaled the RIIb intensity of LSEC. Optical sections with a total area of 6.3mm^2 were analyzed from each of three different mice.

The fluorescence intensities from MR (green) and RIIb (red) channels in the ultra thin sections represented in Fig. 4 were obtained using LSM 510 META software. Randomly selected sinusoids (n=100) from merged color images were cross-sectioned 8 times at 45° angles, and the intensities of both color channels of 8 sections over the LSEC cross-sectional distance from luminal to abluminal surface were recorded. Data were analyzed using a paired *t*-test.

Immunofluoresence from anti-FcRγ-chain (green) was colocalized with signals from mab F4/80 and mab 2.4G2 (Fig. 6) in 60 immunofluorescence optical sections with an area of 12.6mm^2 from a total of 3 mice. Using Olympus FV10-ASW analysis software the Mander's overlap coefficient R was obtained and expressed as a percentage of colocalization(31).

Immunofluorescence signal from mab 2.4G2 colocalized with signal from rabbit anti-RIIb shown in the top row of Fig. 2 was quantified as described for Fig. 6, with the following modification. Individual LSEC (n=60) were cropped from images obtained from two WT livers, and Mander's overlap coefficient was expressed as percent colocalization. By cropping the LSEC we avoided pixels from nuclei non-specifically stained with the rabbit RIIb antibody. Signal from mab 2.4G2 colocalization with immunefluroscence from goat anti-RIIb in individual LSEC (n=194) was quantified manually by scoring the number of LSEC that were positive for 2.4G2 (green) and goat anti-RIIb (red) (Fig. 2 bottom row).

RT-PCR

Total RNA extracted from trizol lysates of organs and cell lines were transcribed to cDNA using Thermoscript RNase H-reverse transcriptase and amplified using primers specific for mouse RIIb. The RNA isolation protocol, primer sequences, and PCR conditions were described earlier(32). The RT-PCR products were resolved by electrophoresis on 1.5% agarose gels, stained with ethidium bromide, and imaged using Quantity One software.

Quantitative precipitin reaction and small immune complex preparation

A single lot of affinity-purified rabbit IgG anti-ovalbumin antibody (Immunology Consultants, Oregon, USA) was 'calibrated' for its interaction with ovalbumin (Sigma) by a quantitative precipitin reaction to derive a point of equivalence (POE)(2, 5, 33). Specifically, microfuge tubes containing serially diluted ovalbumin at concentrations ranging from 6.5μg/ml to 156μg/ml were each incubated with 200μg/ml of rabbit anti-ovalbumin antibody in a total volume of 500μl of PBS at pH 7.4 for 1 hr at room temperature and 18 hrs at 4°C. The mixtures were centrifuged at 2000×g for 10 min; the pellets were dissolved in glycine HCl buffer (0.05M glycine and 0.15M NaCl pH 2.3); and the protein concentrations of pellets and supernatants were determined by UV absorbance at 280nm.

The calibration curve of the precipitin reaction yielded a distinct POE at antigen and antibody concentrations of 26 and 200μg/ml, respectively. To prepare small immune complexes (SIC) for determination of particle size by dynamic light scattering (DLS) and for infusion into mice, we increased the protein concentrations 5-fold greater than the concentration used in the precipitin curve. SIC were prepared by mixing rabbit anti-ovalbumin antibody at 1000μg/ml (~5×200) with ovalbumin (antigen) at 1950μg/ml (26×5×15), a 15-fold excess over the POE antigen concentration determined in the calibration curve, attempting to duplicate the conditions used by others(2, 3, 7). The mixture was incubated for 1hr at room temperature and 18 hrs at 4°C and was centrifuged at 2000×g for 1min. SIC size was measured by DLS. To prepare trace-labeled SIC for infusion into mice, radioiodinated rabbit anti-ovalbumin antibody (iodinated as below) was added to unlabeled antibody at a 1:500 mass ratio prior to mixing antigen with antibody exactly as described above.

Radioiodination of antibody

Affinity purified rabbit IgG anti-ovalbumin antibody was dialyzed against PBS pH 7.4 containing 1.06mM KH_2P0_4, 155mM NaCl and 2.97mM $Na_2HPO_4.7H_2O$ and radioiodinated by a modified chloroglycouril (CGU) method using CGU-coated tubes (Pierce). Briefly, at room temperature 1μCi of $Na^{125}I$ (Pierce) was activated in a CGU-coated tube for 6 minutes, and the activated $Na^{125}I$ was transferred to 100μl of antibody at 1.5mg/ml. The iodination reaction was terminated at 9 min by adding 50μl of 10mg tyrosine/ml in PBS at pH 7.4. The radioiodinated antibody was separated from free radioiodine using PD-10 desalting columns equilibrated with 0.1% fish gelatin in PBS. The precipitability of labeled antibody in 12.5% iced TCA was >95%. Labeling efficiency was ~50%. The cpm/μg of $Na^{125}I$ labeled antibody was 1.4×10^7 and 3.2×10^6 in two experiments.

Analysis of SIC using dynamic light scattering (DLS)

The particle size of SIC was estimated by dynamic light scattering (BI-200SM Research Goniometer System, Brookhaven Instrument Inc., Holtsville, NY) under the following conditions: detection angle 90°C, laser wavelength 633nm, temperature 20°C, measurement duration 2 min. The particles were diluted in 0.22μm-filtered PBS. Fe_3O_4 particles of size range 200–250 (BD Bioscience, USA), 10, and 5nm (NN labs, Fayetteville, USA) were analyzed to check the precision of the instrument and were found to have a mean diameters of 209, 12, and 20nm, respectively; suggesting imprecision at low particle size. The standard

latex particles of size 40, 92, and 100nm were found to have a mean diameter of 42, 93, and 98nm, respectively. The mean diameters by volume of antigen and antibody at a concentration of 1mg/ml were 6±1 and 5±1nm, mean±variance of two observations, respectively. The mean diameter by volume of particles at the POE was 1228±774nm. The mean diameter by volume of SIC particles prepared at a 3-fold excess antigen was measured to be 220±14nm. The characterization of SIC prepared at 15-fold excess antigen are presented in Fig. 7B and the text. All samples showed a mono-dispersed distribution with insignificant outliers and aggregates.

Clearance kinetics of SIC

To characterize *in vivo* SIC clearance kinetics, we infused by tail vein freshly prepared radioiodinated SIC containing 1.4 and 1.9×10^6 cpm in 58μl. Two identical experiments were performed three months apart, in each infusing 3 WT and 3 RIIb KO mice matched for sex and age. The mice were bled *via* the retro-orbital plexus of ~ 15μl blood at post-infusion times of 1, 5, 10, 20, 30 and 60 min. To adjust for different body weights of individual mice, the blood concentrations of radioactive SIC (cpm/10 μl blood) were normalized to an average value of dose/body weight among animals (i.e., a dose of 1.6×10^6 cpm/25.43 g body weight). Since a semi-log plot of blood concentrations of iodinated SIC from both strains indicated biphasic decay, we employed a biexponential decay model to fit the SIC concentration-time profile. Half-lives were calculated by 0.693/-slope, where the slope was obtained from the biexponential decay analysis. Independent two-sample t-test was performed to compare the means of two genotypes. Differences between WT and KO strains were considered significant at $P < 0.05$.

Quantification of SIC in various organs

Mice (n=3) were infused intravenously with freshly prepared radioiodinated SIC containing 1.1×10^6 cpm in 58μl and were sacrificed at 25 min. The mice were bled via the retro-orbital plexus of ~ 20μl; organs (liver, kidney, lung, spleen and heart) were removed and weighed. SIC in the weighed portions of each organ were measured and quantified after factoring total organ weight.

RESULTS

Most RIIb of the mouse is in the liver

We recently noticed that the expression of RIIb on LSEC was astonishingly high, far in excess of what we had perceived to be expressed on other RIIb reservoirs of the body such as spleen, lymph nodes, B cells, and macrophages(12). More precisely, assessing in our mind's eye the brightness and extent of RIIb fluorescence in a microscopic field of view of liver sections, and multiplying this by the 3 dimensions of the liver, the body's largest internal organ, the total quantity of RIIb would be far higher than any of the other RIIb sites of the body (not shown). It has long been known that a like assessment of the human liver with a specific anti-RIIb antibody gives the identical impression by immunolabeling (14). Quantifying our visual impression, we measured by immunoblotting the expression of RIIb in lysates of the liver and spleen and most of the other major organs and tissues of the body (Fig. 1). Consistent with our visual impression, we found that of the total body pool of RIIb,

fully 72 ± 5% (n = 3) was expressed in the liver while the remaining 28% was spread among the other organs and tissues of the body, each being less than 10%. By mobility of the anti-RIIb identified bands, the liver appeared to express mostly the b2 protein isoform but also some b1, whereas, as expected, most of the RIIb in spleen was b1 (Fig. 1A). Our immunoblots of organ lysates affirm that this RIIb KO strain shows no evidence for the RIIb bands (not shown). The band with b1 mobility in the kidney lane, as well as unidentified bands at 75 and 45 kD in many lanes were artifact based upon their presence in tissues from RIIb KO mice (not shown). Further studies of kidney tissue sections examined by IF microscopy with three anti-RIIb antibodies showed no evidence for the expression of RIIb in the kidneys (not shown).

Because our method of quantifying tissue expression of proteins from band densities in immunoblots entailed a large multiplication factor for liver due to its relative size, we also measured the expression of the tyrosine kinase Syk, reasoning that a molecule expressed largely in the spleen would appear highly expressed in liver if our method were artifactually amplifying the extent of liver expression(34). Confirming the validity of our method, 63 ± 6% of total body Syk was expressed in the spleen but less than 10% in liver and all other organs except the ilium (13%) where B cells and macrophages are prevalent (Fig. 1B).

LSEC expression of RIIb confirmed with three anti-RIIb antibodies

Within the liver, RIIb is predominantly expressed in LSEC(12, 14, 17, 35). We confirmed this conclusion by IF microscopy using three anti-RIIb antibodies, i.e., mab 2.4G2 and two polyclonal antibodies from goat and rabbit, the last directed toward the cytoplasmic tail sequence of RIIb. We found that all three antibodies gave similar and mostly overlapping signals in LSEC (Fig. 2); these signals were specific for RIIb in that liver sections from RIIb KO mice showed no LSEC binding (not shown). None of these antibodies gave positive signals with endothelium of portal and hepatic veins. All three antibodies showed a weak staining pattern with KC as we reported earlier for mab 2.4G2(12).

Within the liver most RIIb is in LSEC

We quantified by IF microscopy of liver sections the relative expression of RIIb between LSEC and KC by colocalizing the binding of two anti-RIIb antibodies with the KC marker F4/80 (Fig. 3). We found that of the total liver RIIb pixel intensity, 90% was expressed in LSEC and 10% in KC.

RIIb expression in LSEC predominates toward the apical membrane

Having earlier found that RIIb in the endothelium of the human placenta is expressed in the interior of the cell and not at the plasma membrane(28), we employed the same strategy to localize RIIb in mouse LSEC, examining ultra thin (<100 nm) sections of liver by 3-color IF microscopy, comparing anti-mannose receptor (MR) binding, which is relatively specific for LSEC(12), with anti-RIIb antibody binding (Fig. 4A). Quantifying the pixels of the two colors in merged images (Fig. 4B), we concluded that, unlike its localization in human placental endothelium, RIIb does not predominate in the interior of the cell; rather it appeared to be more highly expressed toward the apical portion of the LSEC, while MR was more diffusely spread throughout the cell.

The RIIb mRNA isoform expressed in liver is b2

Having found that LSEC-expressed RIIb constitutes nearly all RIIb of liver (Fig. 3), we realized that we could easily determine the mRNA isoform of RIIb in LSEC by RT-PCR analysis of whole liver mRNA, comparing band sizes with known sizes from RIIb-expressing cells characterized earlier by others. Such an experiment indicated that the predominant isotype in liver was b2 with only a trace band of b1 being seen in the agarose gels (Fig. 5). We have analyzed the published cDNA sequence of rat RIIb from LSEC that was not isotyped in the original publication and find that the isotype was b2 and not b1(17). Thus, human, rat, and mouse RIIb, which are highly expressed in LSEC, are of the b2 isotype. (14, 16, 17)

FcRγ-chain is expressed only in KC and not in LSEC

We were unable to determine with confidence whether other members of the FcγR family were expressed in LSEC because of a dearth of reliable antibodies to RI, RIII, and RIV that would be useful in IF microscopy. However, since all three of these agonist receptors require for function the association of the FcRγ-chain(36–38), we realized that by assessing FcRγ expression in LSEC we could indirectly assess the expression of the agonist members of the FcγR family in mouse. By 3-color IF microscopy we found FcRγ to be expressed only in the KC of the liver and not in the LSEC (Fig. 6A). Quantifying the colored signals in these images, we affirmed that FcRγ was a distinctive feature of KC and not LSEC (Fig. 6B). Thus, it seems likely that RI, RIII, and RIV are not expressed in LSEC.

Quantitative precipitin curve and SIC characterization

We prepared SIC using a quantitative precipitin curve described 76 years ago by Heidelberger(5). Calibrating a single lot of affinity-purified rabbit IgG anti-ovalbumin antibody we determined the concentrations of antibody and ovalbumin at the point of equivalence (POE) where the immune complexes precipitated maximally (Fig. 7A). We then prepared SIC at a concentration of antigen 15-fold greater than the POE concentration, conditions found by others to yield SIC(2, 3, 5). Measured by dynamic light scattering these SIC had a mean diameter by volume of approximately 39 nm with a range from 20 – 150 nm (Fig. 7B).

SIC are not cleared efficiently in the RIIb KO mouse strain

Testing a prediction of our central hypothesis, that the RIIb of LSEC serves the purpose of removing SIC from circulation, we measured the elimination rate of SIC from the blood stream of both WT and RIIb KO strains. Mice were infused by tail vein with trace-radioiodinated SIC prepared at 15x antigen excess, as described above; the decay of γ-irradiation from peripheral blood was followed over the course of 1 hr; and the data in cpm were plotted in semi-logarithmic fashion (Fig. 8). Indeed, our prediction was not falsified. Rather, we found that the rate of SIC clearance from the RIIb KO strain was dramatically retarded compared with the WT strain. Specifically, both curves described biexponential decay with early and late phases. Decay was most obvious during the late phase, from 10 – 60 min, where half-lives were 87 ± 20 min and 367 ± 222 min for WT and KO mice, respectively (mean ± sd, n = 5 – 6, $P = 0.0001$), indicating a 3-fold lengthier survival of SIC

in the absence of RIIb. In contrast, decay rates during the early 1 – 5 min period were not statistically different between the two strains, half-lives for WT and RIIb KO strains being 12 ± 6 min and 19 ± 10 min, respectively (n = 5 – 6, $P = 0.2$) (Fig. 8). Note also that the cpm at 1-min were >20% lower in WT compared with the KO strain (see Discussion).

Quantification of SIC in various organs

Documenting that infused SIC homes mostly to liver, we autopsied 3 mice 25 minutes after infusion of radioiodinated SIC. Of the total administered dose we recovered 72 ± 2% in blood, 27± 2% in liver, 0 ± 1% in lung, 1± 0% in spleen, and 0 ± 1% in kidney (mean ± sd). Thus, nearly all of the cleared SIC (96%) was found in the liver.

DISCUSSION

Our results allow two major conclusions. First, RIIb is highly expressed on the endothelial cells of the liver sinusoids. This impression is easily reached by simple inspection of a section of liver stained with anti-RIIb antibody. But, wanting to quantify our visual impression we have measured by immunoblotting the amount of RIIb expressed in the major organs of the body and have concluded that the fraction of total RIIb on LSEC is astonishingly high, about three-quarters of the total RIIb in the body. Relatively small fractions of the total are noted in spleen and blood and bone marrow. It should be acknowledged that we have not sampled all organs, so our total value may be somewhat underestimated, but in fact we have sampled all of the major immune system organs and would conclude that the liver content is far in excess of any other organ.

The second major conclusion to be derived from our data is that RIIb of the liver sinusoidal endothelium is responsible for removing SIC from blood. This follows from our observation that the elimination rate of SIC from blood of the RIIb KO strain was severely diminished. Three elements of this conclusion require comment. First, we contend that the liver is the major organ removing SIC. This contention is supported by our observations 1) that the RIIb KO mouse is severely deficient in eliminating SIC, 2) that the majority of RIIb of the mouse is expressed in the liver, and 3) that in our hands 96% of cleared SIC is found in the liver by direct γ-counting. Further, the literature supports this conclusion with abundant direct data showing liver clearance of the major fraction of blood-borne SIC (1, 3, 4, 15, 39, 40). The spleen, contrary to common wisdom, is only a minor participant in SIC elimination.

The second element of our conclusion deserving comment is that RIIb is the operant FcγR responsible for liver clearance. This observation is remarkable because this receptor has been known almost exclusively as an inhibiting receptor, down modulating the immune complex-mediated effects of the other agonist receptors in its gene family. By contrast, here in our studies it functions as an agonist. Early work, however, indicated that it was indeed capable of agonist activity, specifically, of pinocytic uptake of ligand; but these were *in vitro* experiments and not *in vivo* as ours are (41–43). We know of one other situation where this receptor appears to act alone, without an associated receptor, and that is to produce apoptosis when clustered on B cells (44). The mechanistic details of how RIIb acts on LSEC to eliminate immune complexes will require further study.

The third remarkable element of our major conclusion is that a specialized endothelium, the LSEC, is the predominant cell responsible for SIC elimination in that 90% of liver RIIb is expressed on LSEC. The LSEC, according to the literature, is a vigorous scavenger of blood stream detritus, expressing a variety of surface receptors for blood-borne material, displaying abundant coated vesicles and lysosomes appropriate for a disposal mechanism(45), and in our hands eliminating blood-borne virus with remarkable efficiency(12). Further, the uptake of IC by LSEC has been well documented by others (4, 13, 16, 46). We note parenthetically that FcγR-expressing endothelium has been found elsewhere only in the human placenta, and there too the isoform expressed is RIIb(28).

The absence of the small fraction (10%) of total liver RIIb expressed on KC cannot be responsible for the slow rate of immune complex elimination in the RIIb KO mouse. Rather, the absence of RIIb on KC would be predicted to render the KC more vigorously endocytic due to overactive agonistic FcγR unopposed by the inhibitory RIIb. The result would be a more rapid decay of blood-borne SIC in the KO strain compared with the WT strain, the exact reverse of what we found.

We find the decay kinetics of SIC in the RIIb KO strain noteworthy on two accounts. First is the striking decrease in the rate of elimination during the latter of the two biexponential elimination phases, from 5 – 60 min, indicating that RIIb is largely responsible for the removal of blood-borne SIC. Second is the observation that the 1-min point on the WT curve is >20% lower than the 1-min point of the KO curve ($P = 0.002$, Fig. 8) despite the strains being matched not only for age and sex but adjusted for radioisotope dose and body weight; and, further, that the period from 1 to 5 min shows similar rates of decay in both strains. We interpret these kinetics to suggest that during the first minute after infusion the LSEC RIIb become saturated with SIC that pinocytose into (likely) coated vesicles, disappearing from the LSEC surface such that for the next 5 minutes no more RIIb-specific elimination occurs. Then, after 5 minutes, RIIb begin to reappear on the LSEC surface, either by re-expression of endocytosed receptor, suggested by others(16), or by biosynthesis; and an ongoing elimination of SIC ensues at a vigorous rate (half-life ~ 90 min). This supposition suggests a fruitful path of insight into the mechanism of elimination and warrants detailed investigation.

We call attention to old observations that the repetitive infusion of SIC, such as those used here in our study, causes serum sickness with characteristic microscopic findings of glomerulonephritis(6, 7, 47). We speculate that LSEC RIIb, mediating the elimination of SIC, may critically attenuate the manifestations of serum sickness. One would further anticipate that a strain of mouse lacking only LSEC RIIb may be more susceptible to serum sickness and other soluble immune complex-mediated diseases, whereas targeted elimination of RIIb in B cells and myeloid cells would not produce like effects. Likewise, animals harboring mutants of the RIIb gene that result in diminished or defective receptor expression may as well be more susceptible to immune complex-mediated diseases. Such mutants have been described although their analyses appear to have focused on B cell and myeloid RIIb expression, whereas the evaluation of RIIb expression on LSEC would be expected to reveal more telling results(20, 48, 49).

Summarizing for clarity, risking oversimplification, we would propose that SIC are constitutively eliminated by LSEC RIIb, but when this capacity is overwhelmed, the escaping immune complexes become large and lodge in end organs to result in disease. Alterations in the expression and function of RIIb would modify this course of events.

Acknowledgments

The authors are grateful to Dr. Sara Cole, Richard Montione, Brian Kemmenoe, and the staff at The OSU Campus Microscopy and Imaging Facility for training and advice; to Dr. John Cambier, University of Colorado, and Dr. Mark Coggeshall, Oklahoma Medical Research Foundation, for antibodies against mouse RIIb.

This work was supported in part by NIH grant R01 HD38764

ABBREVIATIONS

SIC	small immune complex
RIIb	FcγRIIb
FcγRIIb	Fcγ receptor of the IIb subclass
LSEC	liver sinusoidal endothelial cells
KC	Kupffer cells
DIC	differential interference contrast
and IF	immunofluorescence
WT	wild type
KO	knockout
POE	point of equivalence
DLS	dynamic light scattering

References

1. Benacerraf B, Sebestyen M, Cooper NS. The clearance of antigen antibody complexes from the blood by the reticulo-endothelial system. J Immunol. 1959; 82:131–137. [PubMed: 13631241]
2. Arend WP, Sturge JC. Composition and biologic properties of soluble IgG-anti-IgG immune complexes: Effects of variations in the specificity of rabbit antibodies to different structural components of human IgG. J Immunol. 1979; 123:447–454. [PubMed: 448156]
3. Kurlander RJ, Ellison DM, Hall J. The blockade of Fc receptor-mediated clearance of immune complexes in vivo by a monoclonal antibody (2.4G2) directed against Fc receptors on murine leukocytes. J Immunol. 1984; 133:855–862. [PubMed: 6736648]
4. Skogh T, Blomhoff R, Eskild W, Berg T. Hepatic uptake of circulating IgG immune complexes. Immunology. 1985; 55:585–594. [PubMed: 4018843]
5. Heidelberger M, Kendall FE. A quantitative theory of the precipitin reaction: III. The reaction between crystalline egg albumin and its homologous antibody. J Exp Med. 1935; 62:697–720. [PubMed: 19870443]
6. Dixon FJ, Vazquez JJ, Weigle WO, Cochrane CG. The pathogenesis of serum sickness. Arch Path. 1958; 65:18–28.
7. McCluskey RT, Benacerraf B, POTTER JL, Miller F. The pathologic effects of intravenously administered soluble antigen-antibody complexes. I. Passive serum sickness in mice. J Exp Med. 1960; 111:181–194. [PubMed: 13773804]

8. Haakenstad AO, Striker GE, Mannik M. The disappearance kinetics and glomerular deposition of small-latticed soluble immune complexes. Immunology. 1982; 47:407–414. [PubMed: 7129526]
9. Wener MH, Mannik M. Mechanisms of immune deposit formation in renal glomeruli. Springer Semin Immunopathol. 1986; 9:219–235. [PubMed: 3544280]
10. Hebert, LA.; Birmingham, DJ.; Cosio, FG.; Sedmak, DD. Circulating Immune Complexes. In: van Oss, CJ.; van Regenmortel, MHV., editors. Immunochemistry. Marcel Dekker, Inc; New York: 1994. p. 653-680.
11. Ravetch JV, Clynes RA. Divergent roles for Fc receptors and complement in vivo. Annu Rev Immunol. 1998; 16:421–432. [PubMed: 9597136]
12. Ganesan LP, Mohanty S, Kim J, Clark KR, Robinson JM, Anderson CL. Rapid and Efficient Clearance of Blood-borne Virus by Liver Sinusoidal Endothelium. PLoS Pathog. 2011; 7:e1002281. [PubMed: 21980295]
13. Muro H, Shirasawa H, Takahashi Y, Maeda M, Nakamura S. Localization of Fc receptors on liver sinusoidal endothelium. A histological study by electron microscopy. Acta Pathol Jpn. 1988; 38:291–301. [PubMed: 3134796]
14. Pulford K, Ralfkiaer E, Macdonald SM, Erber WN, Falini B, Gatter KC, Mason DY. A new monoclonal antibody (KB61) recognizing a novel antigen which is selectively expressed on a subpopulation of human B lymphocytes. Immunol. 1986; 57:71–76.
15. Kosugi I, Muro H, Shirasawa H, Ito I. Endocytosis of soluble IgG immune-complex and its transport to lysosomes in hepatic sinusoidal endothelial-cells. Journal of Hepatology. 1992; 16:106–114. [PubMed: 1484143]
16. Mousavi SA, Sporstol M, Fladeby C, Kjeken R, Barois N, Berg T. Receptor-Mediated Endocytosis of Immune Complexes in Rat Liver Sinusoidal Endothelial Cells Is Mediated by FcRIIb2. Hepatology. 2007; 46:871–884. [PubMed: 17680646]
17. March S, Hui EE, Underhill GH, Khetani S, Bhatia SN. Microenvironmental regulation of the sinusoidal endothelial cell phenotype *in vitro*. Hepatology. 2009; 50:920–928. [PubMed: 19585615]
18. Ahmed SS, Muro H, Nishimura M, Kosugi I, Tsutsui Y, Shirasawa H. Fc receptors in liver sinusoidal endothelial cells in NZB/W F1 lupus mice: A histological analysis using soluble immunoglobulin G-immune complexes and a monoclonal antibody (2.4G2). Hepatology. 1995; 22:316–324. [PubMed: 7541388]
19. Nimmerjahn F, Ravetch JV. Fc-receptors as regulators of immunity. Adv Immunol. 2007; 96:179–204. [PubMed: 17981207]
20. Smith KGC, Clatworthy MR. FcγRIIB in autoimmunity and infection: evolutionary and therapeutic implications. Nature Reviews Immunology. 2010; 10:328–342.
21. Takai T, Ono M, Hikida M, Ohmori H, Ravetch JV. Augmented humoral and anaphylactic responses in FcγRII-deficient mice. Nature. 1996; 379:346–349. [PubMed: 8552190]
22. Ganesan LP, Wei G, Pengal RA, Moldovan L, Moldovan N, Ostrowski MC, Tridandapani S. The serine/threonine kinase Akt Promotes Fc gamma receptor-mediated phagocytosis in murine macrophages through the activation of p70S6 kinase. J Biol Chem. 2004; 279:54416–54425. [PubMed: 15485887]
23. Raab M, Kappel S, Kramer A, Sanhaji M, Matthess Y, Kurunci-Csacsko E, Calzada-Wack J, Rathkolb B, Rozman J, Adler T, Busch DH, Esposito I, Fuchs H, Gailus-Durner V, Klingenspor M, Wolf E, Sanger N, Prinz F, Angelis MH, Seibler J, Yuan J, Bergmann M, Knecht R, Kreft B, Strebhardt K. Toxicity modelling of Plk1-targeted therapies in genetically engineered mice and cultured primary mammalian cells. Nat Commun. 2011; 2:395. [PubMed: 21772266]
24. Cao G, Clark RS, Pei W, Yin W, Zhang F, Sun FY, Graham SH, Chen J. Translocation of apoptosis-inducing factor in vulnerable neurons after transient cerebral ischemia and in neuronal cultures after oxygen-glucose deprivation. J Cereb Blood Flow Metab. 2003; 23:1137–1150. [PubMed: 14526224]
25. Rondinelli RH, Epner DE, Tricoli JV. Increased glyceraldehyde-3-phosphate dehydrogenase gene expression in late pathological stage human prostate cancer. Prostate Cancer Prostatic Dis. 1997; 1:66–72. [PubMed: 12496918]

26. Pikula, S.; Pikula, JB.; Awasthi, S.; Awasthi, YC. Differential staining of human erythrocyte membrane proteins by coomassie and silver: Implications in the assessment of homogeneity of membrane proteins. 12. 1996. p. 237-243.
27. Takizawa T, Suzuki K, Robinson JM. Correlative microscopy using FluoroNanogold on ultrathin cryosections. Proof of principle. J Histochem Cytochem. 1998; 46:1097–1102. [PubMed: 9742065]
28. Takizawa T, Anderson CL, Robinson JM. A novel FcγRII receptor-defined, IgG-containing, compartment in placental endothelium. J Immunol. 2005; 175:2331–2339. [PubMed: 16081803]
29. Mori M, Ishikawa G, Takeshita T, Goto T, Robinson JM, Takizawa T. Ultrahigh-resolution immunofluorescence using untrathin cryosections: subcellular distribution of caveolin-1 and CD31 in human placental endothelial cells. J Electron Microsc. 2006; 55:107–112.
30. Takizawa T, Robinson JM. Correlative microscopy of ultrathin cryosections in placental research. Methods Mol Med. 2006; 121:351–369. [PubMed: 16251754]
31. Manders EMM, Verbeek FJ, Aten JA. Measurement of Co-localization of objects in dual-colour confocal images. J Microscopy. 1993:375–382.
32. Mohanty S, Kim J, Ganesan LP, Phillips GS, Hua K, Jarjoura D, Hayton WL, Robinson JM, Anderson CL. IgG is transported across the mouse yolk sac independently of FcγRIIb. J Reprod Immunol. 2010; 84:133–144. [PubMed: 20015554]
33. Maurer, PH. Precipitation reactions. In: Williams, CA.; Chase, MW., editors. Methods in Immunology and Immunochemistry. Academic Press; New York London: 1971. p. 1-58.
34. Duta F, Ulanova M, Seidel D, Puttagunta L, Musat-Marcu S, Harrod KS, Schreiber AD, Steinhoff U, Befus AD. Differential expression of spleen tyrosine kinase Syk isoforms in tissues: Effects of the microbial flora. Histochem Cell Biol. 2006; 126:495–505. [PubMed: 16708245]
35. Muro H, Shirasawa H, Maeda M, Nakamura S. Fc receptors of liver sinusoidal endothelium in normal rats and humans. Gastroenterology. 1987; 93:1078–1085. [PubMed: 3308622]
36. Wirthmueller U, Kurosaki T, Murakami MS, Ravetch JV. Signal transduction by FcgammaRIII (CD16) is mediated through the gamma chain. J Exp Med. 1992; 175:1381–1390. [PubMed: 1314888]
37. Miller KM, Duchemin A-M, Anderson CL. A novel role for the Fc Receptor gamma subunit: enhancement of FcgR ligand affinity. J Exp Med. 1996; 183:2227–2233. [PubMed: 8642332]
38. Nimmerjahn F, Bruhns P, Horiuchi K, Ravetch JV. FcRIV: A Novel FcR with Distinct IgG Subclass Specificity. Immun. 2005; 23:41–51.
39. Haakenstad AO, Mannik M. The disappearance kinetics of soluble immune complexes prepared with reduced and alkylated antibodies and with intact antibodies in mice. Lab Invest. 1976; 35:283–292. [PubMed: 134176]
40. Finbloom DS, Plotz PH. Studies of reticuloendothelial function in the mouse with model immune complexes: I. Serum clearance and tissue uptake in normal C3H mice. J Immunol. 1979; 123:1594–1599. [PubMed: 479594]
41. Miettinen HM, Rose JK, Mellman I. Fc receptor isoforms exhibit distinct abilities for coated pit localization as a result of cytoplasmic domain heterogeneity. Cell. 1989; 58:317–327. [PubMed: 2568890]
42. Miettinen HM, Matter K, Hunziker W, Rose JK, Mellman I. Fc receptor endocytosis is controlled by a cytoplasmic domain determinant that actively prevents coated pit localization. J Cell Biol. 1992; 116:875–888. [PubMed: 1734021]
43. Van Den Herik-Oudijk IE, Westerdaal NAC, Henriquez NV, Capel PJA, van de Winkel JGJ. Functional analysis of human FcγRII (CD32) isoforms expressed in B lymphocytes. J Immunol. 1994; 152:574–584. [PubMed: 8283039]
44. Pearse RN, Kawabe T, Bolland S, Guinamard R, Kurosaki T, Ravetch JV. SHIP recruitment attenuates FcγRIIB-induced B cell apoptosis. Immun. 1999; 10:753–760.
45. Elvevold K, Smedsrod B, Martinez I. The liver sinusoidal endothelial cell: a cell type of controversial and confusing identity. AJP - Gastrointestinal and Liver Physiology. 2008; 294:G391–G400.

46. van der Laan-Klamer SM, Atmosoerodjo-Briggs JE, Hoedemaeker PJ, Hardonk MJ. A histochemical study about the involvement of rat liver cells in the uptake of heterologous immune complexes from the circulation. Histochemistry. 1985; 82:477–482. [PubMed: 4030402]

47. Benacerraf B, Patter JL, McCluskey RT, Miller F. The pathologic effects of intravenously administered soluble antigen-antibody complexes. II. Acute glomerulonephritis in rats. J Exp Med. 1960; 111:195. [PubMed: 19867169]

48. Stefanescu RN, Olferiev M, Liu Y, Pricop L. Inhibitory Fc gamma receptors: From Gene to Disease. J Clin Immunol. 2004; 24:315–326. [PubMed: 15163888]

49. Su K, Yang H, Li X, Li X, Gibson AW, Cafardi JM, Zhou T, Edberg JC, Kimberly RP. Expression Profile of Fc{gamma}RIIb on Leukocytes and Its Dysregulation in Systemic Lupus Erythematosus. J Immunol. 2007; 178:3272–3280. [PubMed: 17312177]

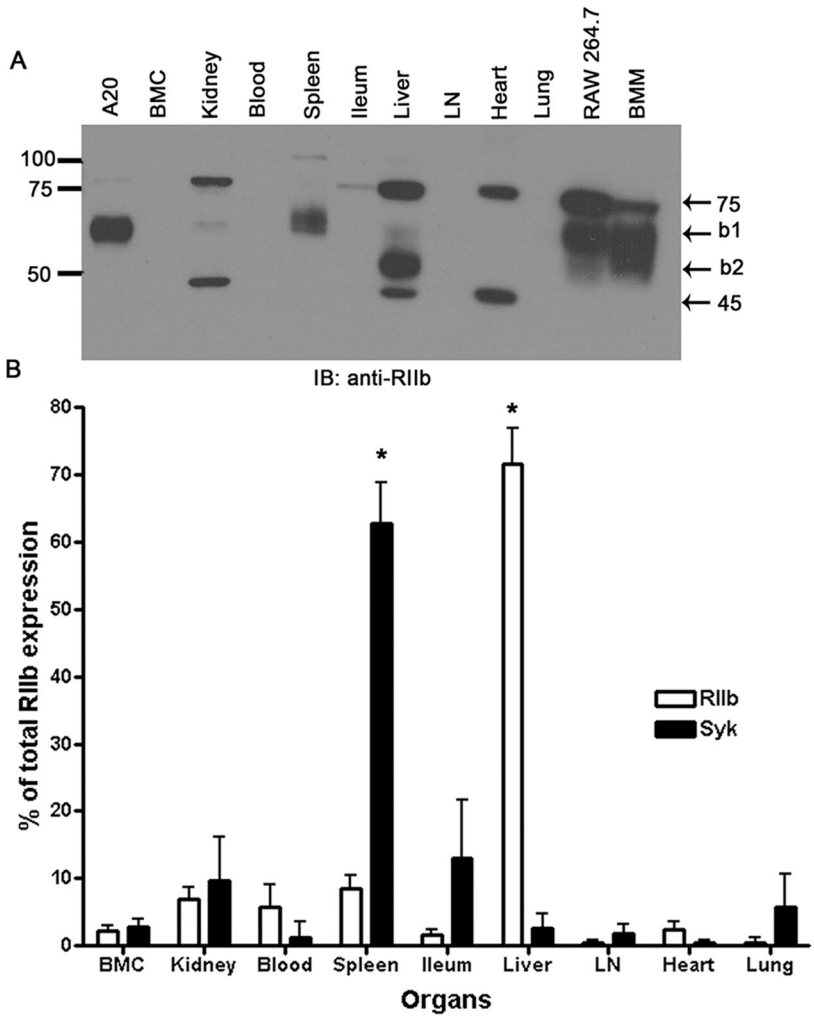

Figure 1. Most RIIb of mouse is in liver

A. An ECL-developed immunoblot using rabbit anti-mouse RIIb antibody showing RIIb expression in several tissue and cell lysates prepared as described in M&M. Numbers are MW markers in kDa. **B.** Bar graph expressing the means and standard deviations of immunoblot-derived band densities, after factoring total organ weight for both RIIb isoforms and Syk from all organs (n=3 WT mice). The asterisks indicate that the expression levels of Syk and RIIb in spleen and liver, respectively, are statistically significantly different from the average of all other organs ($P<0.001$) (See M&M).

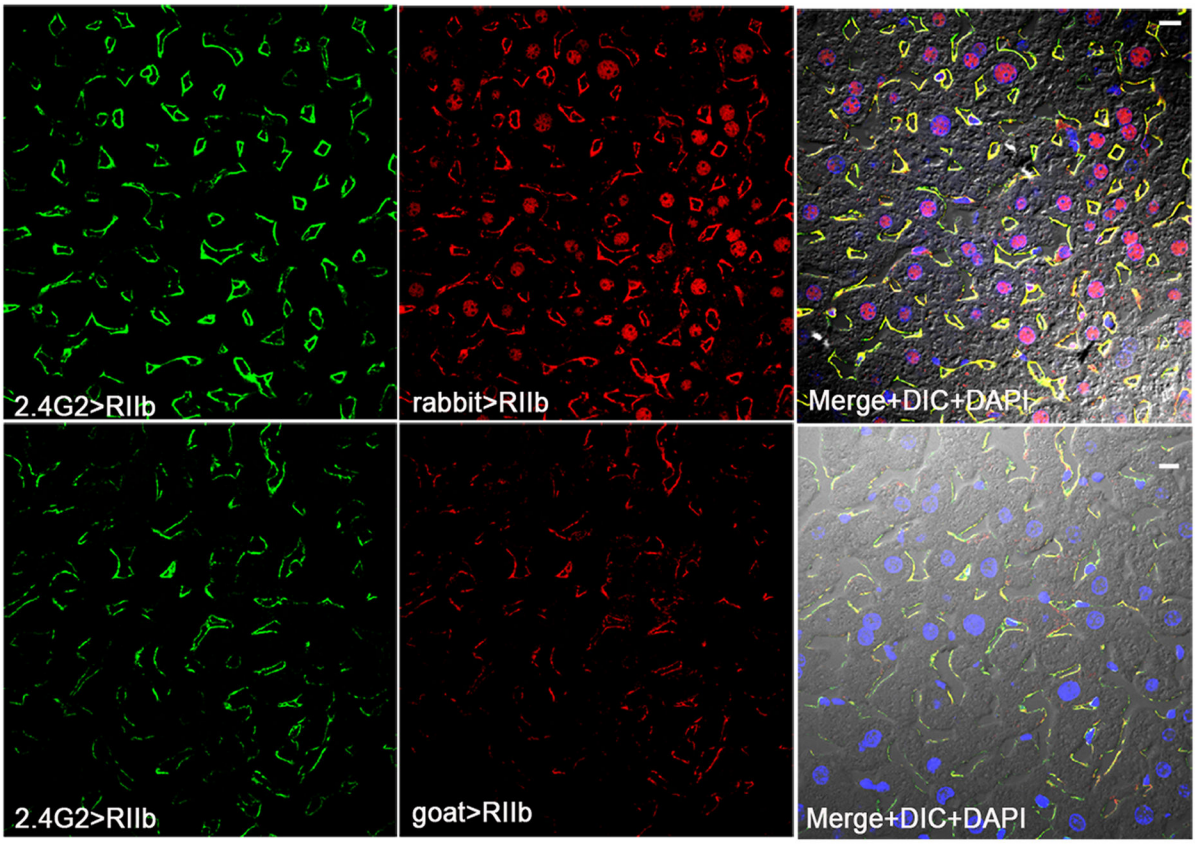

Figure 2. LSEC expression of RIIb confirmed with three RIIb antibodies

The confocal immunofluorescence images in the left column show the binding pattern of anti-RIIb mab 2.4G2 (green). The middle column shows the staining pattern of two anti-RIIb antibodies, rabbit polyclonal anti-mouse RIIb in the first row and goat polyclonal anti-mouse RIIb in the second row (both red). Note in the first row that the nuclei were stained nonspecifically by the rabbit anti-RIIb antibody, as nuclei but not LSEC were stained in liver sections from RIIb KO strain (not shown). The right column shows the merged color images of the left and middle column images plus DIC and DAPI staining of nuclei. The bars in the right column indicate 10μm.

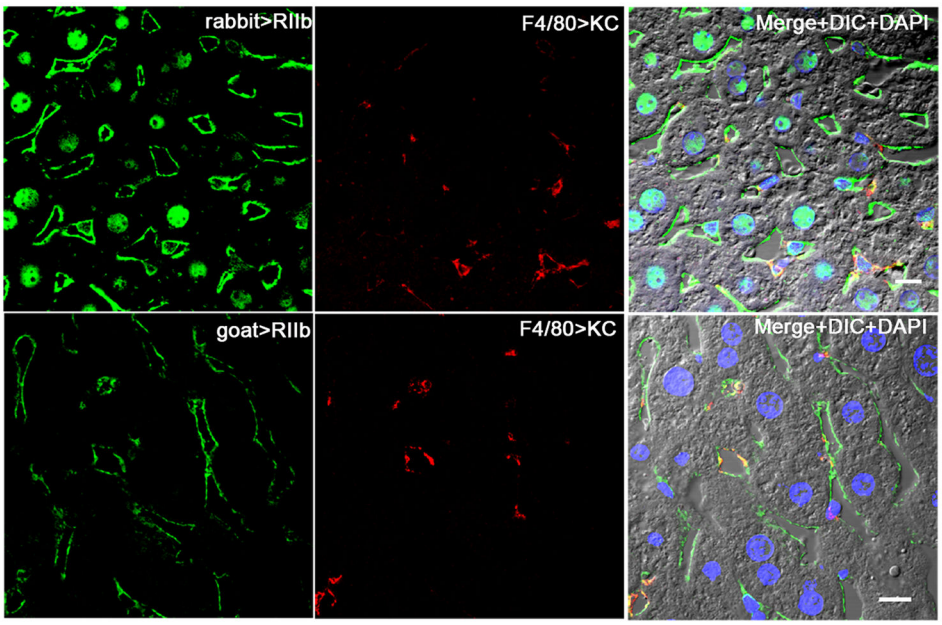

Figure 3. Within the liver most RIIb is in LSEC

Confocal immunofluorescence images in the left column show the binding pattern of rabbit anti-mouse RIIb in the first row and goat anti-mouse RIIb in the second row (both green). In the middle column both rows show KC whereabouts with anti-F4/80 (red). The merged color images in the right column illustrate the relative abundance of RIIb expression in LSEC vs KC and show also DIC and DAPI staining of nuclei. The bars in the right column indicate 10μm.

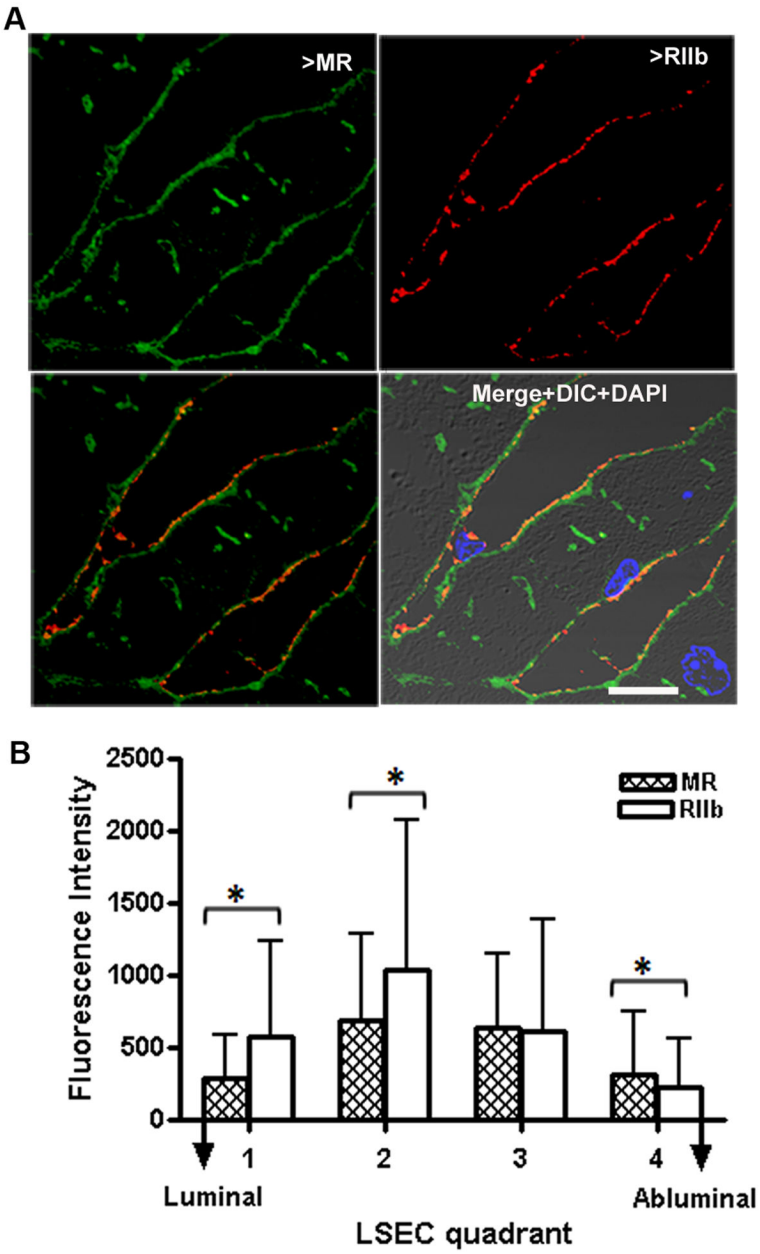

Figure 4. LSEC RIIb is mostly in the membrane

A. 2-color immunofluorescence images of an ultrathin (100μm) cryosection through mouse liver locating the binding of anti-MR (green, upper left) and anti-RIIb (red, upper right). The bottom panels show merged images of the upper two, while the right lower panel adds DIC and DAPI staining. The bar in the merged panel indicates 10μm. **B.** Quantification of relative topological distribution of RIIb and MR in LSEC. The bar graph plots the fluorescence intensities (mean±sd) of the 2 colors in LSEC cross-sections drawn from luminal to abluminal surfaces. n=100 sinusoids. *=P<0.05

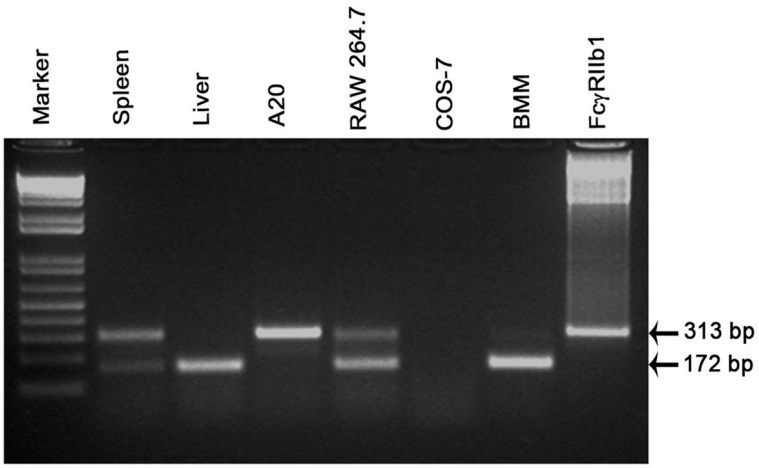

Figure 5. The RIIb isoform expressed in liver is b2

Ethidium bromide-stained agarose gel of electrophoresed RT-PCR products using primers specific for RIIb showing the mRNA expression of the two RIIb isoforms in organs and cells including spleen, liver, A20, RAW 264.7, COS-7, M-CSF differentiated BMM, and b1 cDNA. The two bands at 313 and 172 bp correspond to the two RIIb transcripts b1 and b2, respectively. The data are representative of samples from two sets of WT organs and cell line preparations.

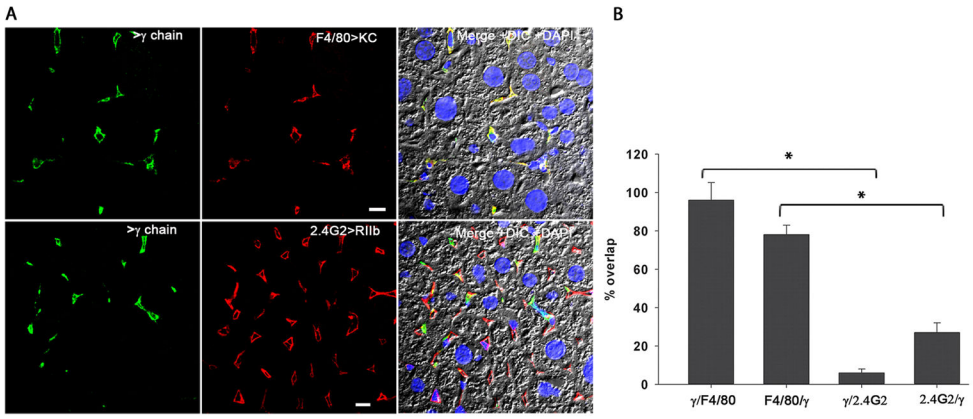

Figure 6. FcRγ-chain is expressed only in KC and not in LSEC

A. The confocal immunofluorescence image in the left column illustrates the expression pattern of γ-chain (green). The middle column shows the location of KC shown using anti-F4/80 (red) in the top row and the location of LSEC using mab anti-2.4G2 (red) in the bottom panel. The merged color image shows the colocalization of signal from γ-chain with signals from F-4/80 and 2.4G2 along with DIC and DAPI staining of nuclei. The bars in the middle column indicate 10μm. **B.** Quantitative colocalization analysis was applied to all images represented in A. The graph represents the percentage of signal from γ-chain antibody (green) colocalizing with signal from F4/80 or 2.4G2 (red) antibody and vice versa in the top panel and also for the bottom panel (mean±sd). Using a random-effects linear regression model the data from bars 1 and 3 and also between bar 2 and 4 were analyzed and the *P*-value was found to be <0.001.

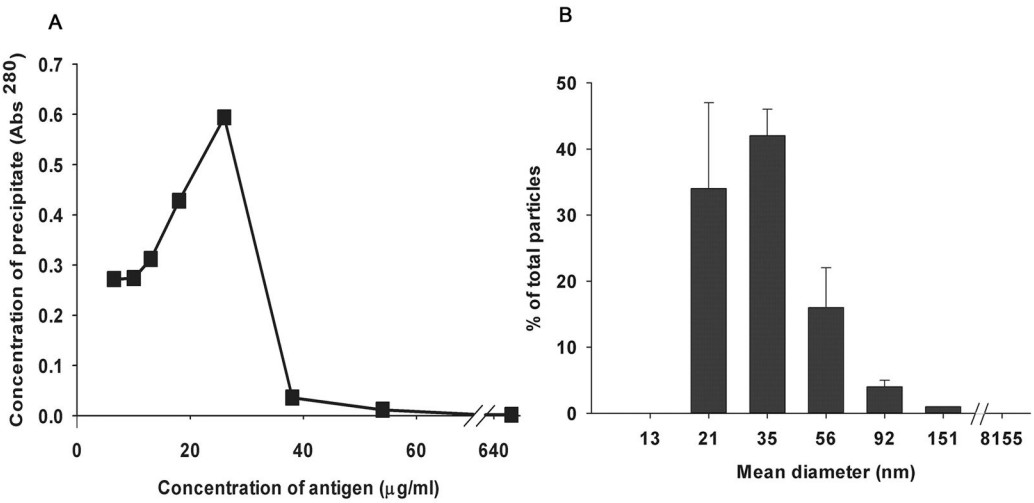

Figure 7. A. Quantitative precipitin curve

The graph shows a quantitative precipitin curve plotting the protein concentrations of immune precipitates (pellets) from a series of tubes incubating increasing concentrations of antigen and a fixed concentration of antibody. The peak marks the POE. **B. Particle size measurement.** Particle size distribution of SIC prepared at a 15-fold antigen excess was measured using DLS; the data obtained with Dynapro software are presented here. The graph plots particle mean (±variance) diameter in nm on the X axis while the Y axis shows the % distribution of total particles calculated using the relative amount of particles (G(d)) at each size.

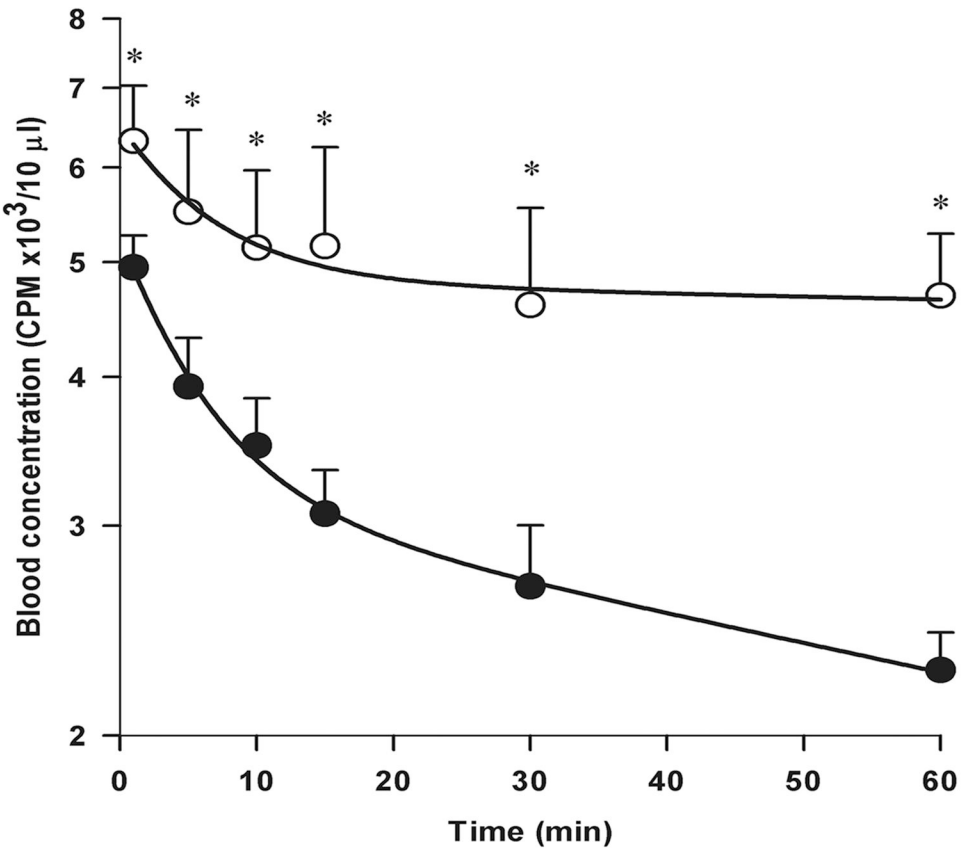

Figure 8. SIC are not cleared efficiently in the RIIb KO mouse strain

We infused via the tail vein radioiodinated SIC prepared at 15x antigen excess of POE and then evaluated the clearance of SIC from peripheral blood by counting γ-irradiation in blood collected from the retro-orbital sinuses. The curve plots mean±sd values of SIC in blood samples, after adjustment for dose/body weight (see M&M), over time from 6 WT (closed circle) and 5 RIIb KO (open circle) animals combining all data from two experiments done three months apart. Asterisks signify statistically significant differences between strain values at each time point, $P<0.05$, using Student's *t*-test.